Postharvest Biology and Technology 139 (2018) 115–126

Contents lists available at ScienceDirect

Postharvest Biology and Technology

journal homepage: www.elsevier.com/locate/postharvbio

Detection of fungal infections in strawberry fruit by VNIR/SWIR hyperspectral imaging

Anna Siedliska[a,*], Piotr Baranowski[a], Monika Zubik[a], Wojciech Mazurek[a], Bożena Sosnowska[b]

[a] Institute of Agrophysics, Polish Academy of Sciences, Doświadczalna 4, 20-290, Lublin, Poland
[b] Department of Biotechnology, Microbiology and Human Nutrition, University of Life Sciences, Skromna 8, 20-704, Lublin, Poland

ARTICLE INFO

Keywords:
Fungal infection
Hyperspectral imaging
Strawberry fruit
B.cinerea
C.acutatum

ABSTRACT

Early stages of fungal infections in strawberry fruit are difficult to detect by the majority of commonly used manual and automatic sorting methods In this study, hyperspectral imaging was applied for detection of fungal infections causing fruit spoilage. Fruit of two cultivars: 'Senga Sengana' and 'Honeoye', were individually inoculated with pathogenic fungi of *Botrytis cinerea* and *Collatotrichum acutatum*, while non-inoculated fruit were used as a control. The reflectance spectra of fruit were acquired during four days after inoculation. Based on the second derivative of the original spectra, 19 wavelengths were selected as the most appropriate for discrimination of infections in strawberries and were used to construct supervised classification models. Among all the studied classifiers, the best prediction accuracies for discriminating fungi species were obtained by using the backpropagation neural network (BNN) model. The accuracy of distinguishing between inoculated and control fruit was higher than 97%. The method presented in this study also allowed early detection of fungal infection, starting 24 h from inoculation when the symptoms of fungal infection are invisible. Multiple linear regression was used to create total anthocyanin content (AC), soluble solid content (SSC) and total phenolic content (TPC) models. Two wavelengths (681 and 1292 nm) were selected to create the AC model and four wavelengths (705, 842, 1162 and 2239 nm) were indicated as the most suitable for the SSC model. The coefficients of determination of the created models were $R^2 = 0.65$ and $R^2 = 0.85$ for AC and SSC, respectively. The results demonstrated that hyperspectral imaging technique has potential for rapid and non-invasive detection of fungal infection and for predicting and visualizing AC and SSC in strawberry fruit during storage.

1. Introduction

Strawberries (*Fragaria* sp.) are one of the most popular berry fruit in the world. This popularity is attributable to their sweet taste and nutritional values, which include a high content of vitamin C, folate, phenolic constituents and potassium (Skrovankova et al., 2015). Strawberries are widely consumed in fresh and processed form as preserves, jams, or as component of yogurts and ice creams. However, strawberry fruit are characterized by a very short shelf life due to their delicate structure and high metabolic rate during storage, which makes them very susceptible to tissue damage and infections caused by a wide range of phytopathogenic fungi, bacteria and viruses (Pan et al., 2014). The main strawberry pathogen is *Botrytis cinerea*, the causal agent of gray mold, followed by *Rhizopus stolonifera, Mucor spp., Colletotrichum spp.,* and *Penicillinum* spp. (Feliziani and Romanazzi, 2016). Postharvest diseases caused by these pathogens are the result of latent infections that are initiated in the field during the growing season and infections from wounding during harvest and handling operations (Michailides et al., 2009).

Early detection of fungal infected fruit is very important both for producers and consumers. Fungal contamination is especially dangerous in packing houses during storage, transport and marketing procedures because even a very small number of infected fruit can spread the infection to adjacent healthy strawberries. The presence of fungal diseases on fruit surfaces not only causes loss of quality, but also diminishes the safety of the final product. Some fungal genera and species can produce mycotoxins, which cause infections or allergies in susceptible individuals (Gallo et al., 2015).

The traditional methods to detect fungal infection and mycotoxin contamination, like traditional microbiological and/or physicochemical techniques (gas and liquid chromatography, mass spectrometry, spectroscopic techniques), are expensive, time- and labor-consuming, require professional experience and have limited applicability since a limited amount of fruit batches can be tested at a time (Sanzani et al., 2016). The need for safe food has compelled scientists and engineers to develop rapid, non-destructive and economic methods for real-time

* Corresponding author.
E-mail address: asiedliska@ipan.lublin.pl (A. Siedliska).

https://doi.org/10.1016/j.postharvbio.2018.01.018
Received 4 September 2017; Received in revised form 23 January 2018; Accepted 23 January 2018
Available online 15 February 2018

monitoring of various quality parameters of fruit which can be applied for early detection of fungal infection (Brosnan and Sun, 2004). In recent years, a number of non-destructive methods have been applied to inspect biomaterials (Jha, 2015) and detect fungal contamination of various food products such as fruit (Lorente et al., 2015; Gruber et al., 2013), vegetables (Prasad, 2015) and cereals (Siripatrawan and Makino, 2015). Soft x-ray imaging has been used to detect fungal infections in corn with classification accuracy of more than 80% (Pearson and Wicklow, 2006) and in wheat with classification accuracy higher than 90% (Narvankar et al., 2009). This method has a number of disadvantages, including a relatively high cost, the need for radiation shielding and the dangers inherent in using radiation, and the need for high voltage power supplies to generate X-rays (Haff and Toyofuku, 2008). Another technique used for detection of fungal infection has been thermal imaging (Baranowski et al., 2015). Chelladurai et al. (2010) used variations in heating and cooling rates, dependent on the biochemical composition, between healthy and fungal infected tissue to detect fungal infections in wheat. They obtained high classification accuracy of about 96% in identifying fungal infections (*Aspergillus glaucus*, *Aspergillus niger* and *Penicillium* spp.) in stored wheat grains. The main disadvantage of this method is its lack of ability to differentiate between fungal species due to similar temperature profiles of samples infected by different fungal species. Moreover, the potential of using this method for early detection of fungal infection is still under research. Pan et al. (2014) studied the performance of electronic nose in detection of strawberry fruit infected by three common post-harvest fungi belonging to *Botrytis sp*., *Penicillium* sp. and *Rhizopus* sp. at early storage stage. This technique allows to successfully discriminate between healthy and fungal inoculated fruit of three species. The e-nose technique was also used for early detection of biodegradation of oranges colonized by *Penicillium digitatum*. Significant responses were observed after only 24 h of incubation (Gruber et al., 2013). E-nose devices offer many advantages over conventional diagnostic tools such as low operating costs, ease of operation without extensive training required, rapid results and response times, good precision, greater portability and flexibility and high adaptability for specialized applications (Wilson, 2017). However, this method still has some shortages. For example, the combination of multiple sensors leads to difficulty in data processing because of the great difference in their performances. Different environmental factors, especially temperature and humidity, result in sensor drift, which reduces data accuracy and reliability (Gu et al., 2017).

Visible and near infrared (VIS/NIR) spectroscopy is a fast, non-destructive and cost-effective method for collecting spectral information of an object (Senthilkumar et al., 2016), but it provides only averaged spectra of target samples without giving any information about the spatial distribution of the chemical composition. A combination of spectroscopic methods with conventional imaging methods is employed in hyperspectral imaging systems, which use spectral and spatial information from an object, and this is critical for detection of food safety and evaluation of food quality attributes. Most research studies have applied hyperspectral imaging systems in quality assessment of fruit: apples (Siedliska et al., 2014; Baranowski et al., 2012), blueberries (Leiva-Valenzuela et al., 2013), bananas (Rajkumar et al., 2012), and cherries (Siedliska et al., 2017). The VIS/NIR hyperspectral imaging method has been successfully applied to develop models for predicting strawberry quality parameters such as color (Giovannini et al., 2014), firmness (Liu et al., 2014), bruise detection (Tallada et al., 2006), soluble solid content (Ding et al., 2015), water content (ElMasry et al., 2007), ascorbic acid content and phenolic content (Amodio et al., 2017). Furthermore, this technique has been investigated with a view to developing classification models for discrimination between strawberries at different ripening stages (Guo et al., 2016) and coming from different cultivars (Liu et al., 2014).

Recently, hyperspectral imaging has been successfully used in food inspection for detection of fungal contamination. Teena et al. (2014) showed that the hyperspectral imaging system in the range 960 to 1700 nm could detect infections caused by *Aspergillus flavus* at 48 h after inoculation when fungal contamination was invisible. Citrus fruit infected by *Penicillium* genus fungi were subjected to inspection using a hyperspectral imaging system in two different spectral regions (Li et al., 2016). Lorente et al. (2015) applied a hyperspectral imaging system in two spectral regions (650–1050 nm and 1000–1700 nm) for detection of *Penicillium digitatum* fungus in mandarins. The maximum overall classification of 97.8% was obtained by employing factor analysis on the NIR spectra. Yao et al. (2008) used spectral image data for classification of five fungal species (*Penicillium chrysogenum, Fusarium moniliforme, Aspergillus parasiticus, Trichoderma viride, and Aspergillus flavus)*. The obtained results indicated that all the five fungi are highly separable with high classification accuracy of 97.7% using only three narrow bands centered at 743 nm, 458 nm, and 541 nm. Similar results were obtained by Sun et al. (2015) for modeling the growth and discrimination of spoilage fungi in peach fruit, including *Botrytis cinerea*, *Rhizopus stolonifer* and *Colletotrichum acutatum*.

In previous studies, a limited effort had been made to develop methods of early detection of fungal contamination in strawberry fruit using VNIR/SWIR hyperspectral imaging. Therefore, the objective of this study was to determine the efficiency of visible, near and shortwave infrared (VNIR/SWIR) hyperspectral imaging techniques for early detection of two typical spoilage microorganisms, i.e. *B. cinerea* and *C. acutatum*, which are frequently found in postharvest strawberry fruit.

2. Materials and methods

2.1. Fruit material

Strawberries (*Fragaria x ananassa Duch*.) of the cultivars 'Senga Sengana' and 'Honeoye' were collected from a local farm located in the Lublin region, in the south-eastern part of Poland. The cultivars were chosen based on their differences in chemical composition and susceptibility to fungal infections. The 'Honeoye' cultivar is known to be more resistant to *Botritis cinerea* and *Colletotrichum acutatum* infections than 'Senga Sengana' (Daugaard, 1999; Denoyes-Rothan et al., 1999). Fresh fruit were harvested at optimum maturity and brought to the laboratory in a cooler, where they were sorted by visual inspection. Only fruit similar in size and free from any mechanical defects and diseases were selected for the experiment. A total of 2700 berries from both cultivars were used for hyperspectral analysis. Strawberries belonging to each cultivar were divided into three groups. One group was kept as a control (non-inoculated), whereas the other ones were inoculated with *Botrytis cinerea* or *Colletotrichum acutatum* fungi, respectively. Prior to inoculation and analysis, the samples were surface sterilized by immersing in 1% sodium hypochlorite solution for 30 s (Wang et al., 2012). To remove any sodium hypochlorite residue, the samples were then washed three times in sterile distilled water and air dried.

2.2. Inoculation procedure

Two pathogenic fungi, namely *Botrytis cinerea* (BC) and *Colletotrichum acutatum* (CA), were used for inoculation. The fungi were grown on potato dextrose agar (PDA) for two weeks at 23 ± 1 °C. The fungal conidia were scraped from the surface of the agar with a sterile glass rod in a small volume of sterile water and diluted to a concentration of about 10^6 spores mL^{-1}.

During the inoculation, strawberry fruit of the two cultivars were immersed in BC (1×10^6 spores mL^{-1}) or CA (1.5×10^6 spores mL^{-1}) or in sterile distilled water as a control for 30 s and air dried. The viable cell count in spore suspension was estimated by a conventional serial dilution method with surface spreading of dilutions onto plate count agar and was 3.65 × 105 CFU mL-1 in CA and 4.95 × 105 CFU mL-1 BC suspension. During the whole experiment (4 days), healthy and

inoculated fruit samples were stored in dark chambers at 20 ± 1 °C and 85% relative humidity (RH), according to the procedure proposed by Wang et al. (2012) and Guidarelli et al. (2011).

2.3. Hyperspectral imaging system

Hyperspectral images of inoculated and non-inoculated strawberry fruit were acquired using a lab-scale hyperspectral imaging system in a reflectance mode. The system consisted of two linear hyperspectral scanners: a VNIR camera with an ImSpector V10E imaging spectrograph (400–1000 nm) and a SWIR camera with a N25E 2/3" imaging spectrometer (1000–2500 nm) (SPECIM, Finland). The cameras were mounted 40 cm above a conveyor belt with speed regulation. The illumination source for each camera consisted of eight 20 W halogen lamps placed in two opposite frames positioned at an angle of 45° towards the conveyor belt surface. Measurements were performed in a dark room to prevent the influence of external illumination. The speed of the conveyor belt was adjusted during line scanning individually for each camera, to suit differences in spatial resolution and integration time of the cameras. The hyperspectral images obtained during the measurements were recorded using data acquisition software SpectralDAQ ver. 2.1 for SPECIM cameras. Initially, the acquired images were corrected with white and dark references, as described by Baranowski et al. (2013). The corrected images were used to extract spectral information, select effective wavelengths, and develop the method for early detection of fungal infections in fruit.

2.4. Hyperspectral image preprocessing

For each hyperspectral cube of the recorded sequences of strawberry fruit (ten fruit in each sequence), one image with the highest contrast between the fruit and background was selected to create the binary mask of fruit using automatic thresholding. The binary masks of the fruit surfaces were then used to extract regions of interest (ROIs) for all spectral images at wavelengths between 450 nm and 2500 nm. In this study a circular ROI with a size of 3500 pixels was used. From the ROI of each segmented strawberry image, the mean reflectance was computed by averaging over all pixels in the fruit surface image.

2.5. Data pre-treatment

The applied hyperspectral imaging system included reflectance data coming from a wide range of wavelengths, and the complexity of the obtained information had to be addressed at different stages of the analysis. Spectral data contain background information and noises besides sample information. To effectively minimize irrelevant information, including noise and background signal caused by random interference of the instrument or environment, spectral processing, including automatic baseline correction, and derivatives of the spectra were used. Automatic baseline correction was chosen to remove the baseline effects from the spectra which occurred during spectral collection. In order to perform the classification analysis to discriminate between non-infected and infected strawberry fruit, it was necessary to reduce the large number of wavelengths to a smaller number of representative independent variables. To enhance the performance of the classification, the second derivative was calculated using the Savitzky-Golay method (second-order polynominal and 9 smoothing points). The 2nd derivative method is a very effective method to eliminate the slope from the spectrum and enhance spectral differences between samples. The most important wavelengths were selected as the high peaks and low valleys in the second derivative plot. In this way, 19 channels representing independent variables were acquired. The selected wavelengths were then used to develop classification models. Pre-treatment of the spectral data was carried out using Unscrambler X ver. 10.1, CAMO Software, Oslo, Norway.

2.6. Classification algorithms

Two classification experiments were performed on the hyperspectral data of the fruit surface. In each experiment, four different classification methods were tested, including Backpropagation Neural Network (BNN), Random Forest (RF), Naive Bayes (NB), and Support Vector Machine (SVM). A back propagation neural network used in this study is actually a descending slope method to minimize the total square of the output, calculated by the network. It consists of at least three layers of units: an input layer, at least one intermediate hidden layer and one output layer. In this study the sigmoid function was used to calculate outputs for the hidden and also output layers. This function is defined as in equation:

$$f(x) = \frac{1}{1 + e^{-x}}$$

where x is the input to the node. To reduce the mean-square error between the target values and the network outputs the gradient descent was used. The gradient descent back propagation consists of application of a training function which updates weight and bias values according to gradient descent. The training of a network occurs when its weight, net input, and transfer functions are described by derivative functions. The weights and biases are updated in the direction of the negative gradient of the performance function (Kuruvilla and Gunavathi, 2014).

The first experiment was to differentiate between healthy fruit and BC/CA infected fruit. The data sets used in this experiment consisted of 1800 infected fruit belonging to the two studied cultivars (all the stages of fungal infection combined) and 900 healthy fruit from both cultivars. The second classification experiment was performed to distinguish days after inoculation for the two studied types of fungi. In this experiment, two data sets were used. One data set consisted of 900 BC infected fruit, while the other one consisted of 900 CA infected fruit. In both experiments, samples were randomly selected for the test set and the validation set in the ratio 75:25. Only the training data set was used to build the classification model, while the test data set was used to check the model's capability to properly classify new samples. The experiment of learning and testing was repeated 10 times with random data selection (cross validation method). In this study, a supervised learning approach was used to train the classification algorithm. All the classification algorithms were implemented from comprehensive software called the Waikato Environment for Knowledge Analysis, or Weka (Hall et al., 2009). Initially, the majority of available classifiers in these categories were tested on representative groups of training and testing data. Four of them with best prediction accuracies were chosen for comparison (these classifiers are presented in Table 1, together with a general description and the actual parameters determined in this study).

2.7. Reference measurements

The reference parameters, including soluble solid content (SSC), total phenolic content (TPC) and total anthocyanin content (AC), were measured for BC/CA-inoculated and non-inoculated strawberry fruit. Samples for reference measurements were taken every 24 h during four days of the incubation period. SSC was measured using a traditional destructive test. After hyperspectral image acquisition, selected samples (three from each variant of the experiment) were squeezed and the obtained juice was measured using a PAL-BX/RI pocket refractometer (Atago Co., Ltd., Tokyo, Japan). TPC was determined using a sample of the fruit tissue extract (10 g) according to the method reported by Šavikin et al. (2009), calculated based on the gallic acid calibration curve and expressed as milligrams of gallic acid equivalents per 100 g of fresh weight. AC was measured following the procedure described by Tonutare et al. (2014). AC was expressed as milligrams of anthocyanin in 100 g of fresh weight.

Table 1
Chosen features of the classifiers used in the study.

Name of classifier's library	Description of algorithm	Acronym	Chosen parameters of classifier
Multilayer Perceptron	Uses backpropagation neural networks to classify instances	BNN	AutoBuild: true; Learning rate: 0.3; Momentum: 0.2; Training time: 500 Hidden layers = (attribs + classes)/2; Transfer functions hidden/outputs: sigmoid/sigmoid; Learning algorithm: gradient descent
Random Forests	Classifier for constructing a forest of random trees	RF	Debug: false; MaxDepth: 0; Num of Features: 0; Num of Trees: 10; Seed: 1
Naive Bayes	Naive Bayes classifier which uses estimator classes. Numeric estimator precision values are chosen based on analysis of the training data	NB	Use Supervised Discretization: true; Debug: false; Use Kernel Estimator: false
LibSVM	A wrapper class for the libsvm tools. Allows users to experiment with One-class SVM, Regressing SVM, and nu-SVM supported by LibSVM tool	SVM	SVM Type: nu-SVC; Kernel Type: linear; Ny: 0.5; Normalize: true; Probability Estimates: true

2.8. Multiple linear regression models

Multiple linear regression analysis was performed using backward stepwise variable selection procedures to create AC, SSC and TPC models based on selected hyperspectral reflectance data. By using this method, the linear relationship between dependent and independent variables can be successfully modeled. In this research, reflectance values for 19 selected wavelengths were selected as independent variables. Multiple linear regression is based on the least squares. In such a model, the best fit is achieved when the sum of squares of differences between the measured and predicted outputs is minimized (Bardak et al., 2016). Once the multiple regression model was created, it was used to compare predicted and actual values of the modelled attributes. The actual and predicted values of the attributes were plotted to visually evaluate the performance of the models. To quantify the predictive ability of the models, the correlation coefficient (R), F-test and standard error of estimation (STE) were determined. The multiple linear regression analysis was performed in STATISTICA software, version 10, StatSoft Inc., USA.

3. Results and discussion

The first stage of the hyperspectral image analysis of infected and uninfected strawberry fruit was to create simple combinations of reflectance data for the chosen wavelengths of the visible range of the spectrum. Fungal infection symptoms were visible on the surface of fruit of the studied cultivars, based on the RGB combination of three wavelengths, at different times after inoculation for the two studied cultivars.

Fig. 1 shows the RGB (R: 638 nm, G: 549 nm, and B: 458 nm) images of inoculated and non-inoculated fruit after storage at 20 °C and 85% RH for 0, 1, 2, 3 and 4 d. It can be noticed that visual symptoms of gray mold occurred on the 3rd day after inoculation (dai) in case of the 'Senga Sengana' cultivar and on the 4th dai (all infected fruit had characteristic gray spots) for the 'Honeoye' cultivar. In case of CA infected strawberry fruit, brown necrotic anthracnose lesions were slightly visible on the 4th dai in case of the 'Senga Sengana' cultivar. In the control group, no visual changes and no mold growth were observed. During storage, loss of firmness was noticeable in all groups of fruit.

3.1. Spectral characteristics of strawberries

The mean reflectance spectra of strawberry fruit on various days after inoculation (0–4 dai) were calculated by averaging pixels in the ROI area. In order to reduce the high dimensionality of the extracted spectral data and to make the discrimination models for quality classification more robust, the most important wavelengths that give the highest discrimination among inoculated and non-inoculated fruit were selected based on 2ndderivative transformation of the spectra. The 2nd derivative averaged spectra are shown in Fig. 2a and 2b aand 2b. Based on a second derivative transformation of the original spectra, the 19 bands situated at maxima or minima were selected and marked as dotted vertical lines in Fig. 2a and 2b and described in Table 2 together with the assignments of these wavelengths. All selected wavelengths belonged to the VNIR/SWIR region of the spectrum and are related to vibration and combination overtones of the C—H, O—H, and N—H bonds, which are the primary structural components of organic molecules. The regions around 600 nm and 680 nm represent anthocyanin and other pigments which are responsible for fruit color (ElMasry et al., 2007). The peak around 1292 nm was due to the absorption band of the C—H stretching second overtone, which was related to anthocyanin compounds (Chen et al., 2015). Hence, variation at this wavelength is caused by an increase in anthocyanin content in BC and CA inoculated fruit. According to McGlone and Kawano (1998), strawberries, like all fresh fruit, are composed mainly of water, with the second major component being carbohydrates. Due to this fact, strong carbohydrate absorbance bands exist at 705 nm, 920 nm and 1162 nm. The water absorption peaks are observed at 749 nm (O—H second overtone), 964 nm (third overtone of O—H stretching vibration), 1414 nm (O—H stretch first overtone) and 1909 (O—H stretch and O—H deformation) (Williams and Norris, 1987). The peaks at 842 nm and 1846 nm are associated with the O—H stretching vibration of sugar (Baiano et al., 2012). The peaks at 790 nm and 2083 nm are related with combinations of the aromatic C—H and C═C stretching vibration.

3.2. Supervised classification models

Two classification experiments were performed on the hyperspectral data of the fruit surface. The first experiment was to differentiate healthy fruit from BC and CA infected fruit. The final results of the classification models for distinguishing between BC infected, CA infected and non-infected fruit are presented in Table 3. The best prediction accuracy for identifying fungal infection in the 'Senga Sengana'

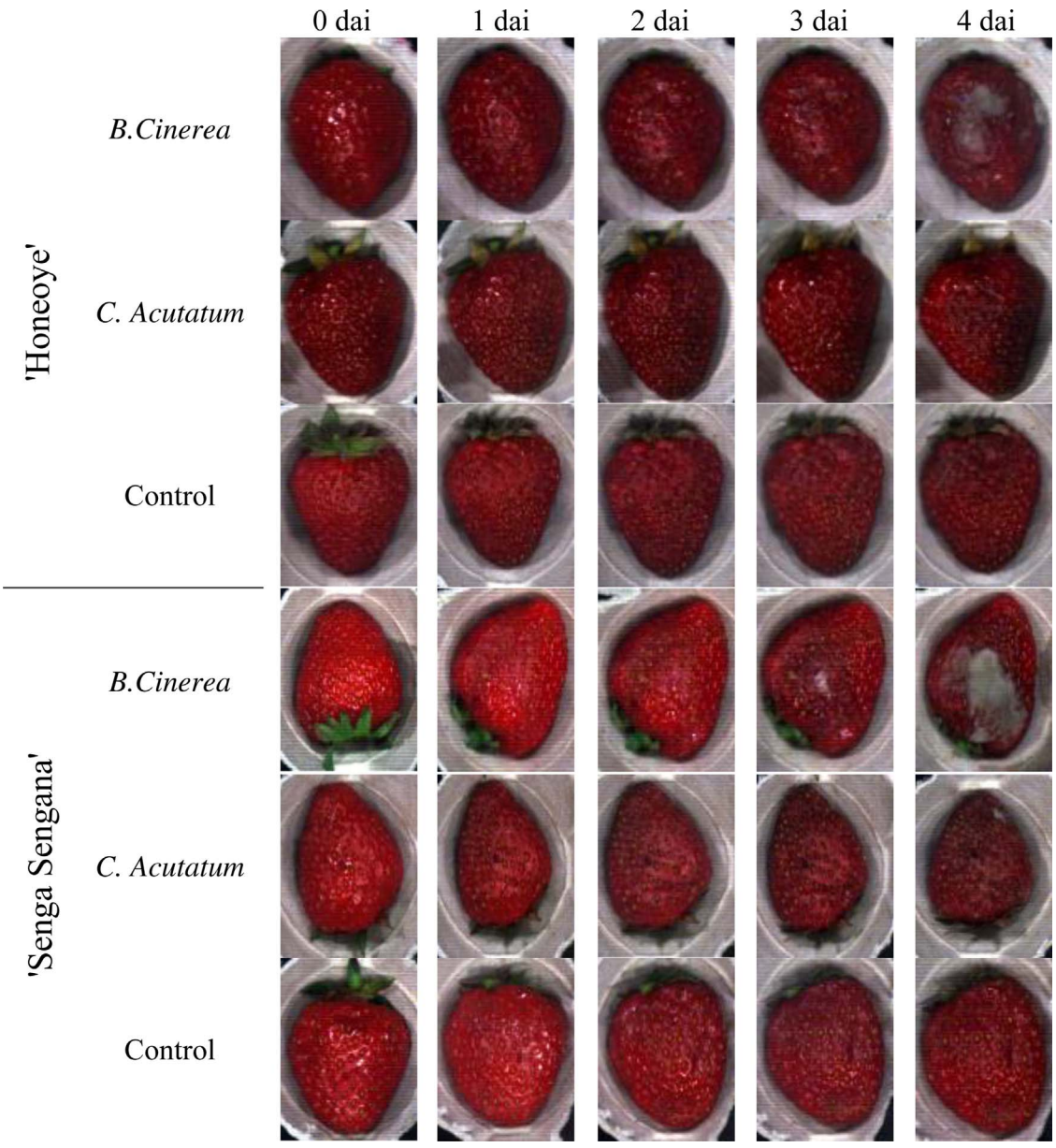

Fig 1. Typical hyperspectral RGB images (R: 638 nm, G: 549 nm and B: 458 nm) of inoculated and non-inoculated strawberry fruit of two studied cultivars studied days after inoculation (dai).

cultivar was obtained for the BNN model (97.2% of correctly classified instances for training and 88.3% for validation sets) and the RF model (96.8% and 85.8% for training and validation sets, respectively). The other models had considerably lower accuracies (the percentage of correctly classified instances ranged 80.1%–93.8% for the training/testing set and 70.0%–85.8% for validation set). In case of the 'Honeoye' cultivar, the obtained classification results were similar and ranged from 80.2% to 88.3% and from 61.7% to 90.0% for the training and validation sets, respectively. The best classification accuracies (88.3% for the training set and 90.0% for the validation set) were obtained for the BNN model. Moreover, it can be seen that the detection precision for BC and CA infected fruit was lower when we took into account both cultivars together. However, also in this case the classification accuracy was still very high (ranging between 69.6% and 87.9% for the training/testing set and 69.6%–86.7% for the validation set). To analyse the performance of the BNN model, which exhibited the highest prediction accuracy among the studied models for detecting the two fungi, and to illustrate how the cases belonged to different classes, the confusion matrices are collected in Fig. 3(a–c). The last column in each matrix shows the prediction accuracy obtained for the discrimination of healthy strawberries from decayed ones. The average accuracy of classification for the control and the two fungal species was 97% and 89% for the 'Senga Sengana' and 'Honeoye' cultivars, respectively (Fig. 3a and 3b). The most probable reason of such accuracy difference was that the 'Honeoye' cultivar is more resistant to fungal infections than 'Senga Sengana'.

A slightly lower discrimination accuracy (88%) for BC, CA, and control group was obtained when both cultivars were studied together (Fig. 3c). The highest classification error occurred when trying to discriminate between BC and CA infected fruit (both cultivars together). It is important to note that by using the BNN model and 19 selected wavelengths, strawberries can be classified into two classes (healthy and decayed) with a high overall accuracy rate. The percentage of correctly classified instances was 97%, 99%, and 98% for 'both cultivars together', 'Senga Sengana', and 'Honeoye', respectively.

The second classification experiment was performed to distinguish days after inoculation for the two studied types of fungi. The final results of the classification models for distinguishing days after

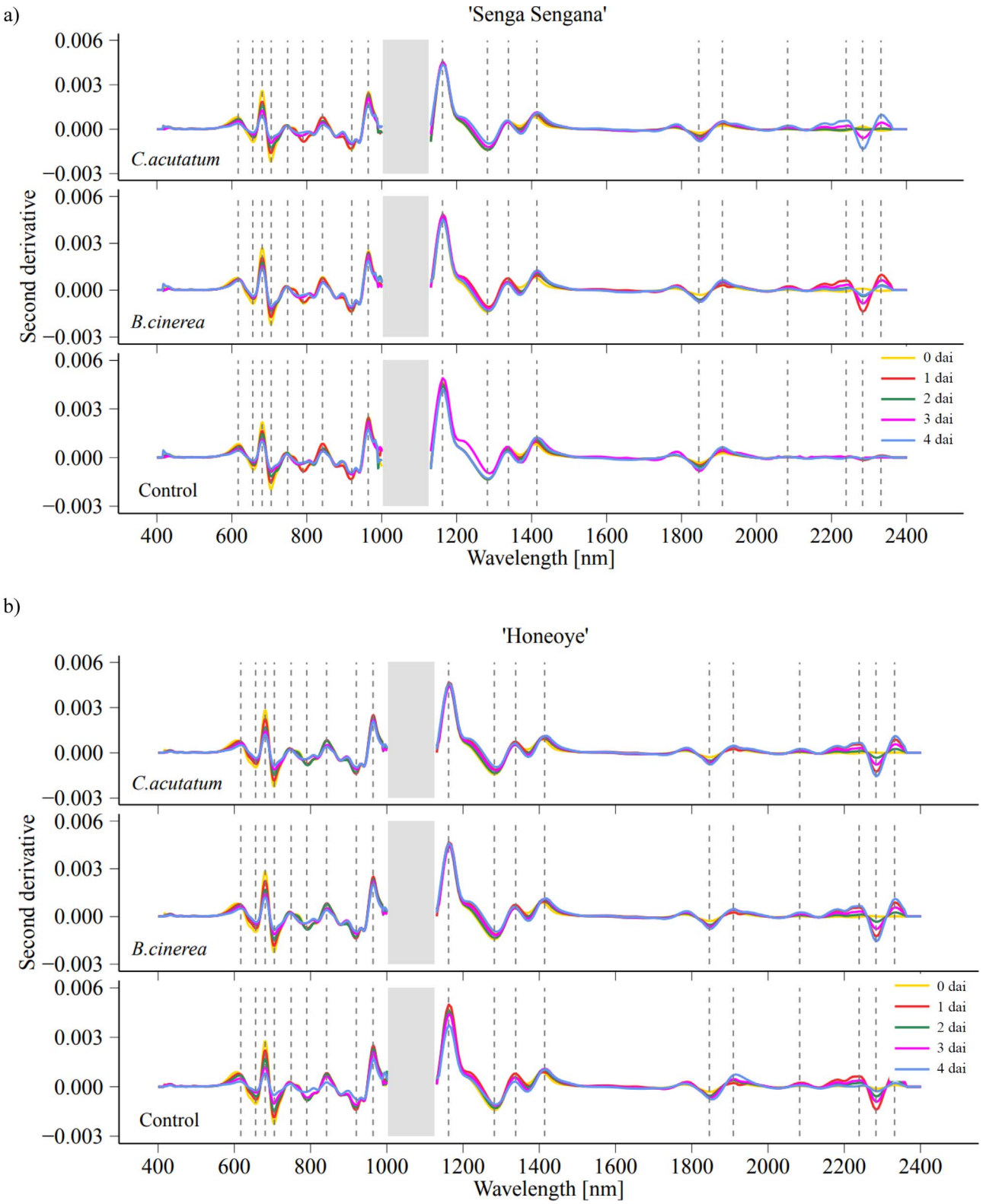

Fig. 2. The second derivative transformed original spectra of inoculated and non-inoculated strawberry fruit of (a) 'Senga Sengana' and 'Honeoye' cultivars. The dotted vertical lines represents the 19 selected bands. The grey area represents the gap region between the VNIR and SWIR cameras.

inoculation are presented in Table 4 and Table 5.

The percentage of correctly classified instances was very high for all the studied models and ranged from 84% to 93% and from 87% to 96% for CA and BC infected fruit, respectively. However, the prediction accuracy obtained for distinguishing the day after inoculation for the BC dataset was slightly higher than for the CA dataset. To illustrate how the cases belonging to different classes were classified by the particular models, the confusion matrices were created. Fig. 4(a–f) presents the confusion matrices for the

BNN model obtained for six variants of the experiment. It can be noticed that the classification results for the 'Senga Sengana' or 'Honeoye' cultivars are considerably higher than for both cultivars

Table 2
The wavelengths selected based on second derivative transformed spectra together with their assignments.

Wavelengths	Assignments
617 nm	Pigments (anthocyanin, carotenoids) absorption bands
656 nm	
681 nm	
705 nm	Carbohydrate absorption band
749 nm	Third overtone of O—H stretching vibrations associated with water
790 nm	Phenolic compounds absorption band
842 nm	Carbohydrate absorption band
920 nm	
964 nm	Second overtone O—H stretching vibrations associated with water
1162 nm	Carbohydrate absorption band
1292 nm	C—H stretching second overtone associated with anthocyanin content
1338 nm	C—H stretching bond
1414 nm	First overtone of O—H stretching vibrations, associated with water
1846 nm	O—H stretching bond, associated with sugar
1909 nm	O—H stretching and O—H deformation, associated with water
2083 nm	Combinations of the aromatic C—H and ring C=C stretching vibration
2239 nm	Carbohydrate absorption band
2283 nm	
2332 nm	C—H stretching bonds

studied together. When distinguishing days after inoculation with the BC fungus, the highest classification error occurred when trying to discriminate between 0th, 1st and 2nd dai. From 3rd dai, the success rate is higher than 97% (Fig. 4a–c). These results confirm that the stage of infection development can be precisely recognised for BC infected fruit and separation between infected and uninfected fruit is possible with great accuracy for different cultivars. It was also noticed that with the development of infection, symptoms are better recognised in reflectance spectra. It was also proven that it is slightly more difficult to discriminate fungal development stages in CA infected fruit (Fig. 4d–f). In this case, the highest number of misclassifications occurred on the 4th dai (18 cases), whereas the lowest number of misclassified cases occurred on the 2nd dai (8 cases). The classification accuracy was least for day 4 in case of CA infected samples. This is probably due to reduced fungal activity on the samples after four days of inoculation. The obtained results were better than those obtained by Sun et al. (2015), who classified correctly 90% of *B.cinerea*, *C.acutatum* and *R stoloifenr* infected peaches at the culture time of 120 h. Using an electronic nose, Pan et al. (2014) obtained discrimination accuracy of 96.6% for fungal infection of strawberry fruit in four groups studied. However, this method has a lot of disadvantages, which include problems with reproducibility, recovery, negative effects of humidity and temperature

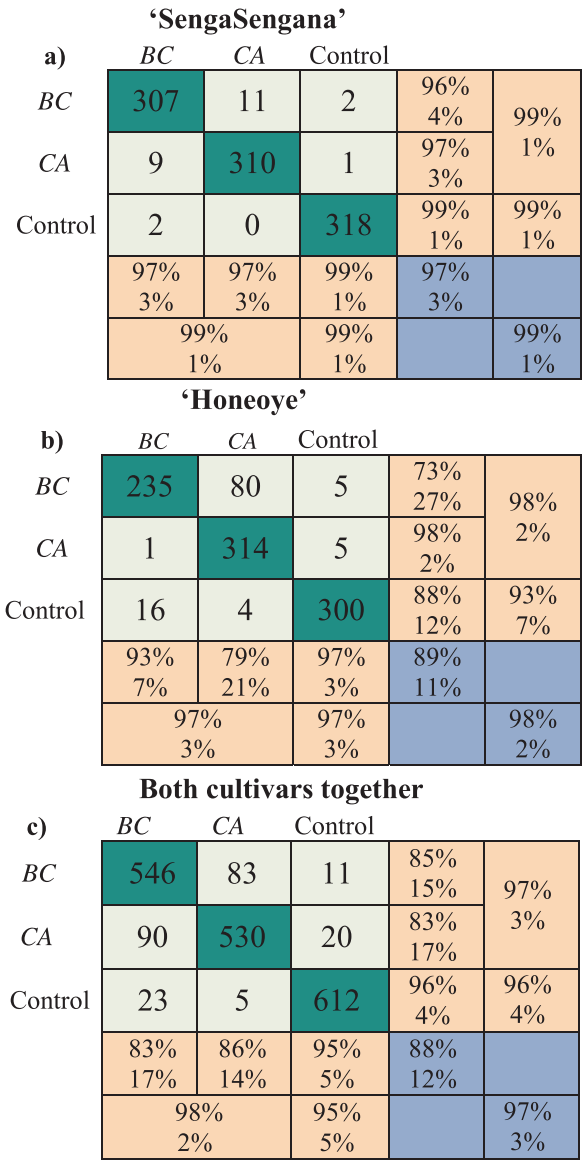

Fig. 3. Confusion matrices obtained for the backpropagation neural network model for distinguishing different fungal species. The last column of the matrix represents the distinction between infected and control fruit.

Table 3
Results of classification models for distinguishing between control and *B.cinerea*, *C.acutatum* infected strawberry fruit.

Cultivar	Classification model	Training/Test set			Validation set		
		Correctly classified instances%	Kappa statistic	Root mean square error	Correctly classified instances%	Kappa statistic	Root mean square error
'Senga Sengana'	BNN	97.2	0.961	0.112	88.3	0.825	0.271
	RF	96.8	0.952	0.145	85.8	0.787	0.264
	NB	89.9	0.848	0.232	85.8	0.788	0.290
	SVM	80.1	0.712	0.313	70.0	0.550	0.374
'Honeoye'	BNN	88.3	0.825	0.237	90.0	0.850	0.224
	RF	84.1	0.770	0.270	88.3	0.825	0.277
	NB	82.5	0.738	0.320	61.7	0.425	0.442
	SVM	80.2	0.700	0.307	78.0	0.670	0.334
Both cultivars	BNN	87.9	0.818	0.258	86.7	0.800	0.288
	RF	85.3	0.779	0.275	74.2	0.613	0.381
	NB	69.6	0.545	0.398	69.6	0.544	0.410
	SVM	72.9	0.593	0.350	62.5	0.437	0.402

Table 4
Results of classification models for distinguishing days after inoculation with the *B.cinerea* fungus.

Cultivar	Classification model	Training/Test set			Validation set		
		Correctly classified instances%	Kappa statistic	Root mean square error	Correctly classified instances%	Kappa statistic	Root mean square error
'Senga Sengana'	BNN	98.2	0.978	0.078	98.0	0.975	0.120
	RF	98.5	0.981	0.079	96.0	0.950	0.157
	NB	98.2	0.978	0.076	94.0	0.925	0.144
	SVM	96.3	0.953	0.122	96.0	0.950	0.157
'Honeoye'	BNN	96.2	0.953	0.119	98.0	0.975	0.156
	RF	96.0	0.952	0.121	96.0	0.950	0.118
	NB	95.2	0.946	0.108	90.0	0.875	0.167
	SVM	96.2	0.953	0.125	94.0	0.925	0.109
Both cultivars	BNN	96.4	0.955	0.111	88.0	0.850	0.192
	RF	96.3	0.951	0.123	89.0	0.862	0.209
	NB	87.5	0.844	0.203	83.0	0.788	0.234
	SVM	89.4	0.867	0.181	83.0	0.776	0.249

Table 5
Results of classification models for distinguishing days after inoculation with the *C.acutatum* fungus.

Cultivar	Classification model	Training/Test set			Validation set		
		Correctly classified instances%	Kappa statistic	Root mean square error	Correctly classified instances%	Kappa statistic	Root mean square error
'Senga Sengana'	BNN	95.0	0.938	0.124	92.0	0.900	0.171
	RF	90.5	0.881	0.163	82.0	0.775	0.245
	NB	87.0	0.838	0.212	88.0	0.850	0.173
	SVM	90.3	0.879	0.171	84.0	0.800	0.233
'Honeoye'	BNN	95.0	0.938	0.123	98.0	0.975	0.074
	RF	93.0	0.912	0.167	86.0	0.825	0.237
	NB	95.0	0.936	0.121	94.0	0.925	0.037
	SVM	94.5	0.936	0.120	96.0	0.950	0.149
Both cultivars	BNN	92.7	0.909	0.151	86.0	0.825	0.215
	RF	92.3	0.905	0.161	86.0	0.825	0.217
	NB	87.0	0.838	0.211	84.0	0.800	0.243
	SVM	79.2	0.739	0.245	79.0	0.738	0.268

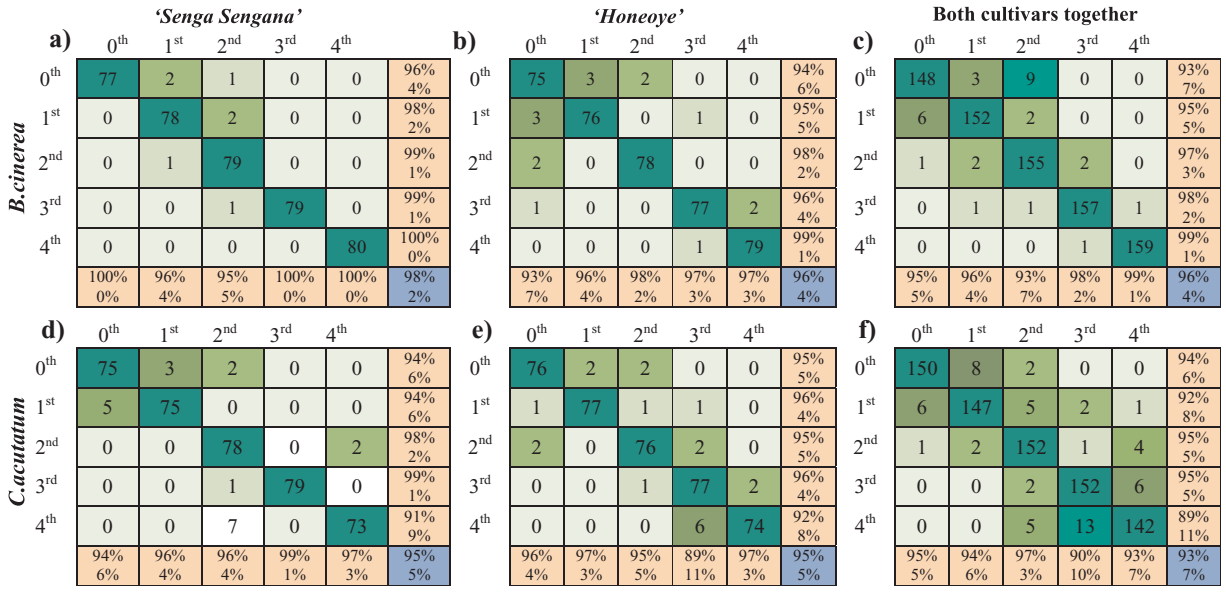

Fig. 4. Confusion matrices obtained for the backpropagation neural network model for the studied days after inoculation (dai).

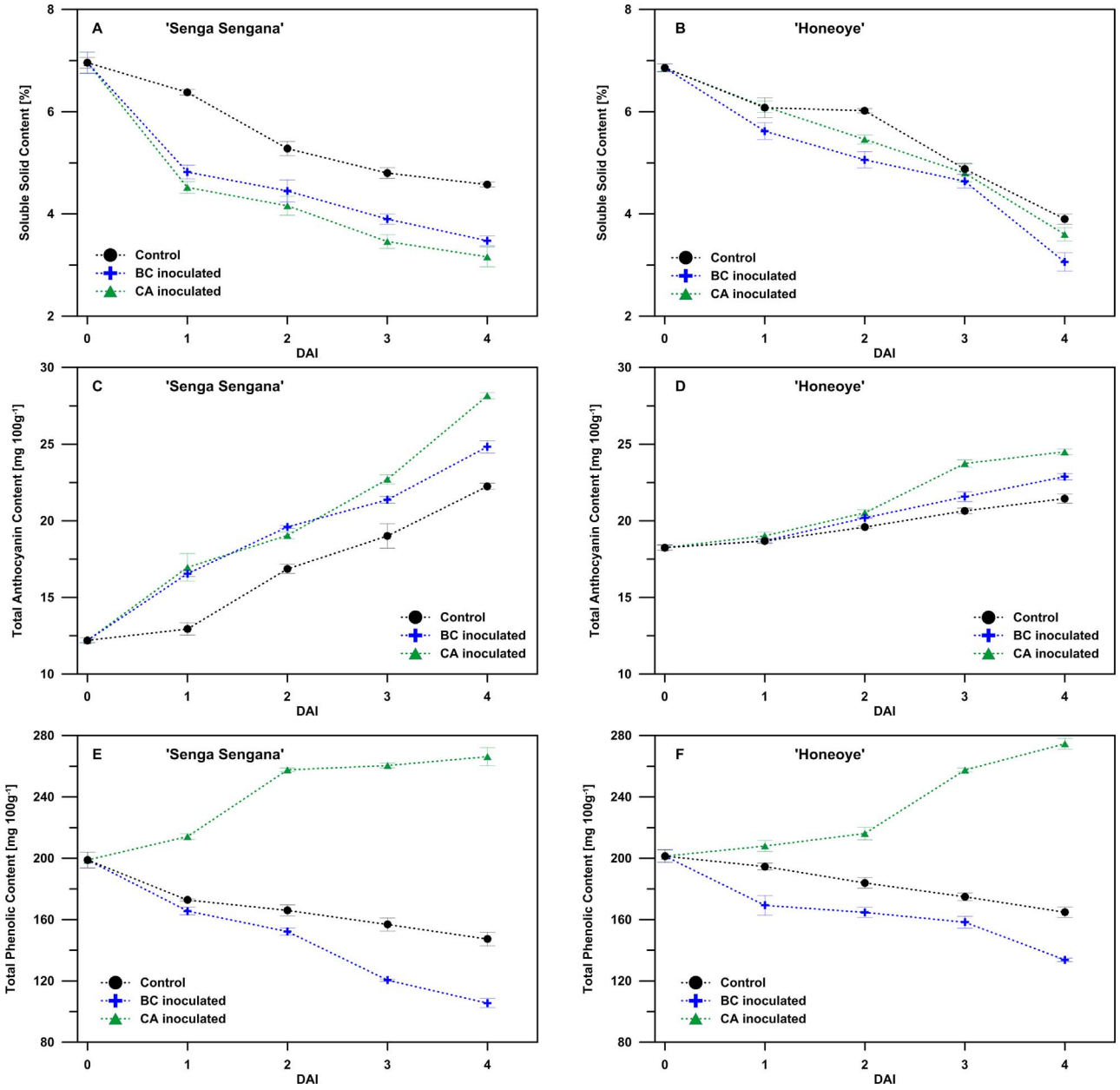

Fig. 5. Changes in (a,b) soluble solid content, (c,d) total anthocyanin content and (e,f) total phenolic content of inoculated and non-inoculated strawberry fruit belonging to 'Senga Sengana' and 'Honeoye' cultivars as function of storage time expressed as days after inoculation (dai). Vertical bars indicate the standard deviation of mean values.

on the sensor responses, and inability to identify individual chemical species with sample gases (Jamal et al., 2010).

3.3. SSC, AC and TPC changes in infected fruit

It was assumed that fungal infection of strawberry fruit caused metabolic changes reflected in differentiation of SSC, AC and TPC in succeeding stages after inoculation. It was interesting to check if these changes can be recognized using hyperspectral data of the fruit surface. Fig. 5 shows the changes in SSC, AC and TPC in fruit of the selected strawberry cultivars, inoculated and non-inoculated with the BC and CA fungi during four days of storage. In general, a decreasing trend was observed in SSC (Fig. 5a and 5b) and an increasing trend in AC (Fig. 5c and 5d) during the whole period of the experiment, both in 'Senga Sengana' and 'Honeoye'. In case of TPC, an ambiguous trend was noticed. The decrease in SSC during four days of storage probably resulted from SSC degradation related to respiration and higher fruit decay, caused by fungal infection (Petrișor et al., 2013). Another interesting observation coming from Figs. 5(a- d) is that in case of the 'Senga Sengana' cultivar there were higher differences in time-dependent SSC and AC between the control and BC/AC variants compared to the 'Honeoye' cultivar. It can be related to the classification results presented in Fig. 3 which show that in the case of 'Senga Sengana' classification accuracy in distinguishing between infected and uninfected fruit was much better than for 'Honeoye'.

The changes in TPC in inoculated and non-inoculated fruit of each cultivar are shown in Fig. 5e and 5f. In this case, an ambiguous trend was noticed. TPC in BC inoculated and control fruit decreased with storage time, while an increase in TPC was observed for CA inoculated fruit, especially during the first two days of storage. However, for both strawberry cultivars the changes in TPC during four days of storage were lowest in non-inoculated fruit. The changes in TPC in fungal infected fruit were caused by metabolic processes resulting from the use of organic acids in the respiratory process (Sogvar et al., 2016).

Table 6
Results of multiple linear regression model for prediction of the total anthocyanin content (AC) and soluble solid content (SSC).

Dependent variable	Independent variables	Regression coefficient	Standard error of regression coefficient	t-student	Summary of the model
Total anthocyanin content (AC)	Intercent	26.74	0.643	41.56	N = 90
	R_{681}	5646.41	822.257	6.87	R = 0.80
	R_{1292}	12037.06	1221.57	9.85	F = 79.45
					STE = 2.27
Soluble solid content (SSC)	Intercent	2.84	0.399	7.10	N = 90
	R_{705}	−1739.32	198.55	−8.76	R = 0.93
	R_{842}	−3908.18	348.84	−11.20	F = 103.29
	R_{1162}	−2026.37	610.19	−3.32	STE = 0.472
	R_{2239}	−9822.00	2641.52	−3.72	

N: number of cases, R: correlation coefficient, F: Snedocor test value, STE: standard error of estimation

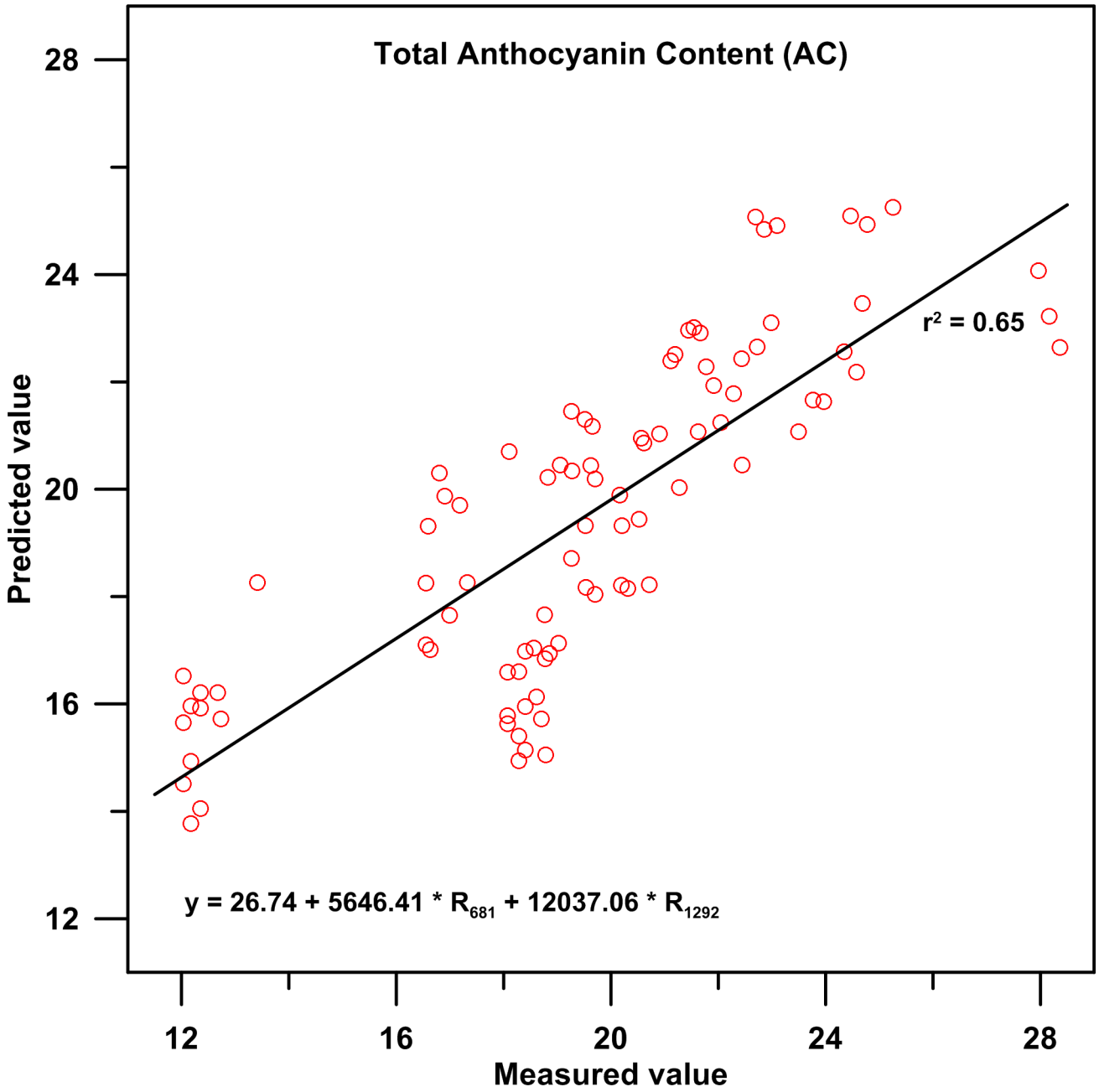

Fig. 6. Relationship between the measured and predicted values of total anthocyanin content calculated using multiple linear regression model.

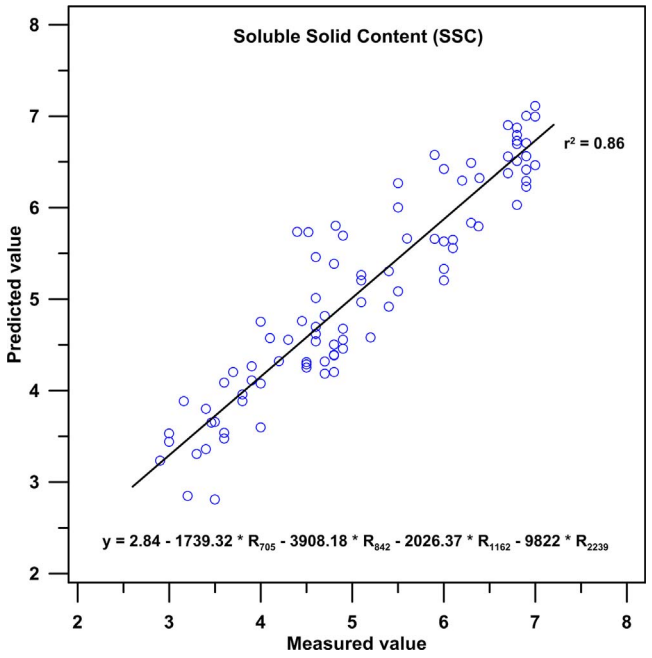

Fig. 7. Relationship between the measured and predicted values of soluble solid content calculated using multiple linear regression model.

3.4. Multiple linear regression models

Because it was confirmed that SSC, CA and TPC change considerably in strawberry fruit during four days after inoculation, it was decided to check if the selected reflectance data from hyperspectral imaging will be suitable to create reliable models for these three parameters. To create AC, SSC and TPC models, multiple linear regression was used with 19 selected wavelengths as independent variables. The backward stepwise approach was applied, in which the independent variables were individually removed until the best model was obtained. The results of multiple regression modelling are presented in Table 6 as well as in Fig. 6 and Fig. 7.

The AC and SSC models include 2 and 4 independent variables, respectively. They represent the pigment absorption band (681 nm) and C−H stretching overtone band (1292 nm) for the AC and carbohydrate absorption bands (705 nm, 842 nm, 1162 nm and 2239 nm) for the SSC model. The summary statistics of these two models indicate a good level of prediction (correlation coefficients R equal to 0.80 and 0.93), and high values of F-test and low values of STE. The high prediction ability of the created models is confirmed by the plots comparing predicted and measured values of two studied parameters (Fig. 6 for AC and Fig. 7 for SSC). The obtained results are comparable with earlier reports on SSC and CA modelling in strawberries. The PLS model of SSC built by ElMasry et al. (2007) on the basis of VIS/NIR (400–1000 nm) reflectance data performed well, with R of 0.85, and the model by Nishizawa et al. (2009), which used spectral data in the 700–925 nm range, had high prediction ability with R of 0.93. Shi et al. (2011) used seven characteristic wavelengths, in the 1135–1322 nm range, to build a multiple linear regression model which reached predictive performance with R of 0.94. Also SWIR (1600–2400 nm) reflectance data of strawberry surface proved sufficient to create a PLS model of SSC with R of 0.89 (Sánchez et al., 2012), similarly to combined VNIR/SWIR (833–2631 nm) used by Guo et al. (2013) to create a synergy interval PLS model based on 1st derivative spectra (R = 0.97). AC modelling was performed in earlier studies based on VNIR reflectance data (400–1000 nm) for strawberries (Kobayashi et al., 2006) and apples (Merzlyak et al., 2003) with the determination coefficient of the anthocyanin content index higher than 0.93. The main advantage of our study is that it revealed the possibility of modelling and determining SSC and AC in case of fungal infection with good precision. It was impossible to create a reliable multiple regression model for TPC based on the 19 selected wavelengths, i.e. the contribution of all the independent variables to the model was too small. It could have been due to the specific behavior of TPC over time in BC and CA inoculated fruit presented in Fig. 5e and 5f. Earlier studies (Lätti et al., 2008; Kljusurić et al., 2016) indicated high variations in phenolic content in different wild berry populations, influenced by environmental conditions, especially the effect of processing and subsequent storage. The differences in metabolic processes after inoculation with the two fungal species studied (BC and CA) caused significant differentiation in TPC, influencing multiple regression modelling.

4. Conclusion

This study aimed to develop a method for early detection of two typical spoilage microorganisms which are frequently found in postharvest strawberry fruit. The obtained results revealed good applicability of hyperspectral imaging in the VNIR and SWIR regions for early detection of *Botrytis cinerea* and *Colletotrichum acutatum* infections on strawberry fruit starting at 24 h from inoculation when fungal contamination is invisible. Thus, the proposed approach is beneficial to avoid cross contamination of fungal infected strawberry fruit with fresh ones and hence could be profitably implemented in fruit handling facilities. However, further work is required to test this technique for other fungal species causing infection.

References

Amodio, M.L., Ceglie, F., Chaudhry, M.M.A., Piazzolla, F., Colelli, G., 2017. Potential of NIR spectroscopy for predicting internal quality and discriminating among strawberry fruit from different production systems. Postharvest Biol. Technol. 125, 112–121.

Baiano, A., Terracone, C., Peri, G., Romaniello, R., 2012. Application of hyperspectral imaging for prediction of physico-chemical and sensory characteristics of table grapes. Comput. Electron. Agric. 87, 142–151.

Baranowski, P., Mazurek, W., Wozniak, J., Majewska, U., 2012. Detection of early bruises in apples using hyperspectral data and thermal imaging. J. Food Eng. 110 (3), 345–355.

Baranowski, P., Mazurek, W., Pastuszka-Woźniak, J., 2013. Supervised classification of bruised apples with respect to the time after bruising on the basis of hyperspectral imaging data. Postharvest Biol. Technol. 86, 249–258.

Baranowski, P., Jędryczka, M., Mazurek, W., Babula-Skowrońska, D., Siedliska, A., Kaczmarek, J., 2015. Hyperspectral and thermal imaging of the response of oilseed rape (Brassica napus) to fungal species of the genus Alternaria. PLoS One 10 (3), e0122913.

Bardak, S., Tiryaki, S., Bardak, T., Aydin, A., 2016. Predictive performance of artificial neural network and multiple linear regression models in predicting adhesive bonding strength of wood. Strength Mater. 48 (6), 811–824.

Brosnan, T., Sun, D.W., 2004. Improving quality inspection of food products by computer vision. J. Food Eng. 61 (1), 3–16.

Chelladurai, V., Jayas, D.S., White, N.D.G., 2010. Thermal imaging for detecting fungal infection in stored wheat. J. Stored Prod. Res. 46 (3), 174–179.

Chen, S., Zhang, F., Ning, J., Liu, X., Zhang, Z., Yang, S., 2015. Predicting the anthocyanin content of wine grapes by NIR hyperspectral imaging. Food Chem. 172, 788–793.

Daugaard, H., 1999. Cultural methods for controlling Botrytis cinerea Pers. in strawberry. Biol. Agric. Hortic. 16 (4), 351–361.

Denoyes-Rothan, B., Lafargue, M., Guerin, G., Clerjeau, M., 1999. Fruit resistance to Colletotrichum acutatum in strawberries. Plant Dis. 83 (6), 549–553.

Ding, X.B., Zhang, C., Liu, F., Song, X.L., Kong, W.W., He, Y., 2015. Determination of soluble solid content in strawberry using hyperspectral imaging combined with feature extraction methods. Guang pu xue yu guang pu fen xi = Guang pu 35 (4), 1020–1024.

ElMasry, G., Wang, N., ElSayed, A., Ngadi, M., 2007. Hyperspectral imaging for nondestructive determination of some quality attributes for strawberry. J. Food Eng. 81 (1), 98–107.

Feliziani, E., Romanazzi, G., 2016. Postharvest decay of strawberry fruit: etiology, epidemiology, and disease management. J. Berry Res. 6 (1), 47–63.

Gallo, A., Giuberti, G., Frisvad, J.C., Bertuzzi, T., Nielsen, K.F., 2015. Review on mycotoxin issues in ruminants: occurrence in forages, effects of mycotoxin ingestion on health status and animal performance and practical strategies to counteract their negative effects. Toxins 7 (8), 3057–3111.

Giovannini, D., Quacquarelli, I., Ranieri, M., Faedi, W., 2014. 2014: Feasibility study of NIR application to strawberry internal fruit quality traits. Acta Hortic. 1049, 947–954.

Gruber, J., Nascimento, H.M., Yamauchi, E.Y., Li, R.W., Esteves, C.H., Rehder, G.P., Shirakawa, M.A., 2013. A conductive polymer based electronic nose for early

detection of Penicillium digitatum in post-harvest oranges. Mater. Sci. Eng.: C 33 (5), 2766–2769.
Gu, X., Sun, Y., Tu, K., Pan, L., 2017. Evaluation of lipid oxidation of Chinese-style sausage during processing and storage based on electronic nose. Meat Sci. 133, 1–9.
Guidarelli, M., Carbone, F., Mourgues, F., Perrotta, G., Rosati, C., Bertolini, P., Baraldi, E., 2011. Colletotrichum acutatum interactions with unripe and ripe strawberry fruit and differential responses at histological and transcriptional levels. Plant Pathol. 60 (4), 685–697.
Guo, Z., Huang, W., Chen, L., Wang, X., Peng, Y., 2013. Nondestructive evaluation of soluble solid content in strawberry by near infrared spectroscopy. In: In: Tan, H. (Ed.), Piageng: Image Processing and Photonics for Agricultural Engineering 8761 SPIE, Sanya, China.
Guo, C., Liu, F., Kong, W., He, Y., Lou, B., 2016. Hyperspectral imaging analysis for ripeness evaluation of strawberry with support vector machine. J. Food Eng. 179, 11–18.
Haff, R.P., Toyofuku, N., 2008. X-ray detection of defects and contaminants in the food industry. Sens. Instrum. Food Qual. Saf. 2 (4), 262–273.
Hall, M., Frank, E., Holmes, G., Pfahringer, B., Reutemann, P., Witten, I.H., 2009. The WEKA data mining software: an update. ACM SIGKDD Explorations Newsletter 11 (1), 10–18.
Jamal, M., Khan, M.R., Imam, S.A., Jamal, A., 2010. Artificial neural network based e-nose and their analytical applications in various field. In Control Automation Robotics Vision (ICARCV). 2010 11th International Conference on IEEE 691–698.
Jha, S.N., 2015. Rapid Detection of Food Adulterants and Contaminants: Theory and Practice. Academic Press.
Kljusurić, J.G., Mihalev, K., Bečić, I., Polović, I., Georgieva, M., Djaković, S., Kurtanjek, Ž., 2016. Near-Infrared spectroscopic analysis of total phenolic content and antioxidant activity of berry fruit. Food Technol. Biotechnol. 54 (2), 236–242.
Kobayashi, T., Nagata, M., Tallada, J., Toyoda, H., Goto, Y., 2006. Study on anthocyanin pigment distribution estimation for fresh fruit and vegetables using hyperspectral imaging: part 2. Visualization of anthocyanin pigment distribution of strawberry (Fragaria Ananasa Duchesne). J. Soc. High Technol. Agric. 18, 50–57.
Kuruvilla, J., Gunavathi, K., 2014. Lung cancer classification using neural networks for CT images. Comput. Methods Programs Biomed. 113 (1), 202–209.
Lätti, A.K., Riihinen, K.R., Kainulainen, P.S., 2008. Analysis of anthocyanin variation in wild populations of bilberry (Vaccinium myrtillus L.) in Finland. J. Agric. Food Chem. 56, 190–196.
Leiva-Valenzuela, G.A., Lu, R., Aguilera, J.M., 2013. Prediction of firmness and soluble solids content of blueberries using hyperspectral reflectance imaging. J. Food Eng. 115 (1), 91–98.
Li, J., Huang, W., Tian, X., Wang, C., Fan, S., Zhao, C., 2016. Fast detection and visualization of early decay in citrus using Vis-NIR hyperspectral imaging. Comput. Electron. Agric. 127, 582–592.
Liu, C., Liu, W., Lu, X., Ma, F., Chen, W., Yang, J., Zheng, L., 2014. Application of multispectral imaging to determine quality attributes and ripeness stage in strawberry fruit. PLoS One 9 (2), e87818.
Lorente, D., Escandell-Montero, P., Cubero, S., Gómez-Sanchis, J., Blasco, J., 2015. Visible?NIR reflectance spectroscopy and manifold learning methods applied to the detection of fungal infections on citrus fruit. J. Food Eng. 163, 17–24.
McGlone, V.A., Kawano, S., 1998. Firmness, dry-matter and soluble-solids assessment of postharvest kiwifruit by NIR spectroscopy. Postharvest Biol. Technol. 13 (2), 131–141.
Merzlyak, M.N., Solovchenko, A.E., Gitelson, A.A., 2003. Reflectance spectral features and non-destructive estimation of chlorophyll carotenoid and anthocyanin content in apple fruit. Postharvest Biol. Technol. 27, 197–1021.
Michailides, T.J., Morgan, D.P., Luo, Y., 2009. Epidemiological assessments and postharvest disease incidence. Postharvest Pathology. Springer, Netherlands, pp. 69–88.
Narvankar, D.S., Singh, C.B., Jayas, D.S., White, N.D.G., 2009. Assessment of soft X-ray imaging for detection of fungal infection in wheat. Biosyst. Eng. 103 (1), 49–56.
Nishizawa, T., Mori, Y., Fukushima, S., Natsuga, M., Maruyama, Y., 2009. Non-destructive analysis of soluble sugar components in strawberry fruit using near-infrared spectroscopy. J. Jpn Soc. Food Sci. 56, 229–235.
Pan, L., Zhang, W., Zhu, N., Mao, S., Tu, K., 2014. Early detection and classification of pathogenic fungal disease in post-harvest strawberry fruit by electronic nose and gas chromatography–mass spectrometry. Food Res. Int. 62, 162–168.
Pearson, T.C., Wicklow, D.T., 2006. Detection of corn kernels infected by fungi. Trans. ASABE 49 (4), 1235–1245.
Petrișor, C., Câmpeanu, G., Delian, E., 2013. Influence of fungicides and antagonistic yeast product on postharvest strawberries quality. Sci. Papers-Series B, Hortic. 57, 219–222.
Prasad, K., 2015. Advances in nondestructive quality measurement of fruit and vegetables. Postharvest Biology and Technology of Horticultural Crops: Principles and Practices for Quality Maintenance 51.
Rajkumar, P., Wang, N., EImasry, G., Raghavan, G.S.V., Gariepy, Y., 2012. Studies on banana fruit quality and maturity stages using hyperspectral imaging. J. Food Eng. 108 (1), 194–200.
Šavikin, K., Zdunić, G., Janković, T., Tasić, S., Menković, N., Stević, T., Đorđević, B., 2009. Phenolic content and radical scavenging capacity of berries and related jams from certificated area in Serbia. Plant Foods Hum. Nutr. 64 (3), 212–217.
Sánchez, M.T., De la Haba, M.J., Benítez-López, M., Fernández-Novales, J., Garrido-Varo, A., Pérez-Marín, D., 2012. Non-destructive characterization and quality control of intact strawberries based on NIR spectral data. J. Food Eng. 110 (1), 102–108.
Sanzani, S.M., Reverberi, M., Geisen, R., 2016. Mycotoxins in harvested fruit and vegetables: insights in producing fungi biological role, conducive conditions, and tools to manage postharvest contamination. Postharvest Biol. Technol. 122, 95–105.
Senthilkumar, T., Jayas, D.S., White, N.D.G., Fields, P.G., Gräfenhan, T., 2016. Near-Infrared (NIR) hyperspectral imaging: theory and applications to detect fungal infection and mycotoxin contamination in food products. Indian J. Entomol. 78, 91–99 special.
Shi, J., Zou, X., Zhao, J., Mao, H., 2011. Selection of wavelength for strawberry nir spectroscopy based on bipls combined with saa. J Infrared Millim. Waves 30, 458–462.
Siedliska, A., Baranowski, P., Mazurek, W., 2014. Classification models of bruise and cultivar detection on the basis of hyperspectral imaging data. Comput. Electron. Agric. 106, 66–74.
Siedliska, A., Baranowski, P., Zubik, M., Mazurek, W., 2017. Detection of pits in fresh and frozen cherries using a hyperspectral system in transmittance mode. J. Food Eng. 215, 61–71.
Siripatrawan, U., Makino, Y., 2015. Monitoring fungal growth on brown rice grains using rapid and non-destructive hyperspectral imaging. Int. J. Food Microbiol. 199, 93–100.
Skrovankova, S., Sumczynski, D., Mlcek, J., Jurikova, T., Sochor, J., 2015. Bioactive compounds and antioxidant activity in different types of berries. Int. J. Mol. Sci. 16 (10), 24673–24706.
Sogvar, O.B., Saba, M.K., Emamifar, A., 2016. Aloe vera and ascorbic acid coatings maintain postharvest quality and reduce microbial load of strawberry fruit. Postharvest Biol. Technol. 114, 29–35.
Sun, Y., Gu, X., Wang, Z., Huang, Y., Wei, Y., Zhang, M., Pan, L., 2015. Growth simulation and discrimination of *Botrytis cinerea*, *Rhizopus stolonifer* and *Colletotrichum acutatum* using hyperspectral reflectance imaging. PLoS One 10 (12), e0143400.
Tallada, J.G., Nagata, M., Kobayashi, T., 2006. Non-Destructive estimation of firmness of strawberries (Fragaria* ananassa duch.) using NIR hyperspectral imaging. Environ. Control. Biol. 44 (4), 245–255.
Teena, M.A., Manickavasagan, A., Ravikanth, L., Jayas, D.S., 2014. Near infrared (NIR) hyperspectral imaging to classify fungal infected date fruit. J. Stored Prod. Res. 59, 306–313.
Tonutare, T., Moor, U., Szajdak, L., 2014. Strawberry anthocyanin determination by differentia spectroscopic method −how to get true results? Acta Scientiarum Polonrum. Hortorum Cultus 13, 35–47.
Wang, Q., Tao, S., Dubé, C., Tury, E., Hao, Y.J., Zhang, S., Khanizadeh, S., 2012. Postharvest changes in the total phenolic content, antioxidant capacity and L-Phenylalanine ammonia-Lyase activity of strawberries inoculated with botrytis cinerea. J. Plant Stud. 1 (2), 11.
Williams, P., Norris, K., 1987. Near-infrared Technology in the Agricultural and Food Industries. American Association of Cereal Chemists, Inc.
Wilson, A.D., 2017. Electronic-nose devices potential for noninvasive early disease-detection applications. Ann Clin Case Rep. 2017 (2), 1401.
Yao, H., Hruska, Z., Kincaid, R., Brown, R.L., Cleveland, T.E., 2008. Differentiation of toxigenic fungi using hyperspectral imagery. Sens. Instrum. Food Qual. Saf. 2 (3), 215–224.